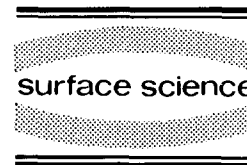




ELSEVIER

Surface Science 311 (1994) 360–374



# Surface phonon dispersion of $p(2 \times 2)\text{O}/\text{Ni}(111)$

G. Tisdale<sup>1</sup>

*Department of Physics and The James Franck Institute, The University of Chicago, 5640 South Ellis Ave, Chicago, IL 60637, USA*

S.J. Sibener<sup>\*,2</sup>

*Department of Chemistry and The James Franck Institute, The University of Chicago, 5640 South Ellis Ave, Chicago, IL 60637, USA*

(Received 4 August 1993; accepted for publication 9 November 1993)

---

## Abstract

Using inelastic electron scattering we have mapped the salient surface phonon features of the  $p(2 \times 2)\text{O}/\text{Ni}(111)$  system along the  $\bar{\Gamma}-\bar{M}'$  direction of the surface Brillouin zone. Because of the diffuse scattering properties of the system, we have developed a maximum entropy deconvolution routine to extract enhanced spectroscopic information from the data. With this routine a set of experimental dispersion curves were successfully obtained for the O/Ni system. We have additionally developed a lattice dynamical model of the system and used spectral density curves from this to produce theoretical dispersion curves for comparison to the experimentally generated curves. From these comparisons we conclude that the bonding interactions in the topmost nickel layers are well described by a scaling relation which relates intermetallic force constants and bond length, and that the various bond lengths present in the surface region can be referenced to a single force constant description of the bulk Ni–Ni interaction. The surface force field derived in this way for  $p(2 \times 2)\text{O}/\text{Ni}(111)$  differs significantly from that of the clean Ni(111) interface.

---

## 1. Introduction

The  $p(2 \times 2)\text{O}/\text{Ni}(111)$  system was one of the first adsorption systems studied by surface scientists and has been studied throughout the past 30 years with a variety of surface sensitive techniques. One of the primary results of these efforts

has been a gradually evolved understanding of the surface structure of the system. In one of the early studies, Marcus et al. [1] studied the system with LEED and the then newly developed dynamical scattering algorithms and concluded that the system was slightly reconstructed. As more refined surface probes have been brought to bear on this system, the picture has gradually changed to include more reconstruction in the top layer of nickel atoms. A recent study by Grimsby et al. [2] once again addresses this system with LEED, but employs more sophisticated scattering computations which have been run on present day supercomputers. Their study concluded that

---

\* Corresponding author. Fax: +1(312)702 5863.

<sup>1</sup> Present address, Qmax, 7642 Plaza Ct., Willowbrook, IL 60521, USA.

<sup>2</sup> 1992/93 Visiting Fellow, Joint Institute for Laboratory Astrophysics, Boulder, CO 80309-0440, USA.

$p(2 \times 2)\text{O}/\text{Ni}(111)$  is significantly reconstructed. Fig. 1a presents their view of the system structure, the one which we shall adhere to in this paper. This reconstruction consists of a twist deformation of three of the top layer nickel atoms, and a vertical displacement of all of the atoms in the top layer of the unit cell.

From the discussion above, it is evident that the oxygen overlayer significantly affects the bonding in the nickel surface. It is natural to wonder how much change the oxygen has induced in the surface bonding as compared to the clean metallic surface. Such changes can be quantified effectively with high resolution electron energy loss spectroscopy (HREELS). During the past decade a variety of studies have employed HREELS to develop simple force constant models of several systems by comparing surface phonon data with lattice dynamical calculations. In this paper we employ surface vibrational spectroscopy to understand the surface force field of the  $p(2 \times 2)\text{O}/\text{Ni}(111)$  system.

In our work we build upon previous vibrational studies of this system. Ibach and Bruchmann [3] have studied  $p(2 \times 2)\text{O}/\text{Ni}(111)$  using low beam energy HREELS and mapped the phonons at the center of the Brillouin zone. Their data have been analyzed by a number of theoretical groups which have modeled the system in a variety of ways. However, all have used their techniques to compute the energies of the phonons at the center of the surface Brillouin zone. Allan et al. [4] have produced a simple electronic structure model which generates surface force constants. They have used this technique in conjunction with slab model calculations to predict phonon energies. Bortolani et al. [5] have treated the  $p(2 \times 2)\text{O}/\text{Ni}(111)$  system as a  $\text{Ni}_3\text{O}$  molecule joined to a  $\text{Ni}(111)$  substrate. They calculate the vibrational energies of their hybrid construction and use these to represent the energies of the surface phonons. Black [6] has used continued fraction techniques to produce one atom spectral densities, which in turn yield phonon energies. Finally, Strong et al. [7] used a slab model with Lennard-Jones potentials to compute spectral density curves and phonon energies. Each of these computations reproduces the significant features

of the experimental data. Additionally, we use the surface phonon measurements of Menezes et al. [8] on  $\text{Ni}(111)$  to provide baseline data for the clean metallic interface.

In this study we have extended the existing literature in two ways. First, we have experimentally mapped the salient phonon modes throughout the surface Brillouin zone along the  $\bar{\Gamma}-\bar{M}'$  direction. Second, we have developed a lattice model incorporating the latest structural information and have used it to theoretically map the surface phonons throughout the surface Brillouin zone, and have in turn used this phonon information to develop a simple model of the chemical bonding in the system.

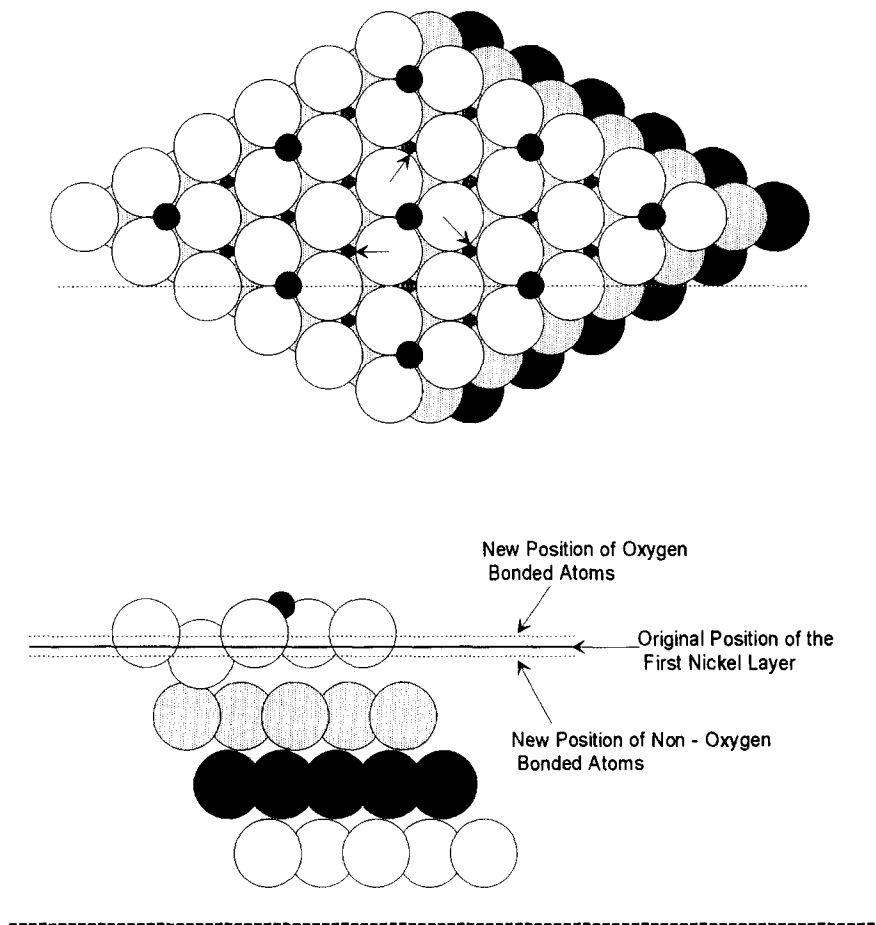
In the following section we present the details of the experiment. Because of the complex domain structure of this system it tends to scatter diffusely and weakly. Consequently we have developed a maximum entropy algorithm for extracting the spectroscopic features from the data. This we detail in Section 3. In Section 4 we discuss the lattice dynamics modeling that we have done, and in Section 5 we present our conclusions.

## 2. Experimental

We performed this set of experiments on a  $\text{Ni}(111)$  crystal which had been cut to within 0.3 deg of the bulk planes; this was checked with X-ray and laser diffractometry. We cleaned the original  $\text{Ni}(111)$  surface with repeated argon sputtering and anneal cycles to 1200 K. The primary contaminant during this procedure was sulfur; which we typically reduced to less than 0.3% of a monolayer. We checked the surface ordering qualitatively with LEED; the reproducible production of HREELS spectra provided the ultimate test of our ordering procedure. The base pressure for the vacuum system was  $8 \times 10^{-11}$  Torr.

The oxygen overlayer was prepared by monitoring the  $(\frac{1}{2}, 0)$  diffraction spot intensity with the rotating analyzer of the HREELS spectrometer. Oxygen was dosed at 300 K until this spot maxi-

a)



b)

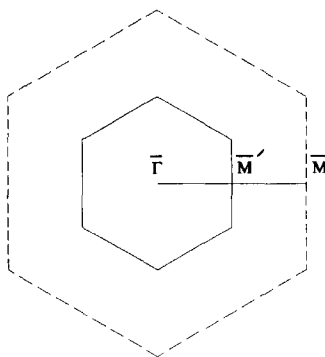


Fig. 1. (a) Schematic views of  $p(2 \times 2)\text{O}/\text{Ni}(111)$ . The upper view presents a view along the surface normal of the oxygen overlayer and the top three nickel layers. The arrows indicate that the three nickel atoms bonded to the oxygen atom are shifted by  $0.07 \text{ \AA}$  along the arrow direction. The lower view shows the surface as cut through the dashed line in the upper figure. Note that the oxygen lifts three of the nickel atoms away from their original bulk positions while the fourth relaxes toward the second layer of nickel atoms. This figure has been adapted from Grimsby et al. [2]. (b) Surface Brillouin zones for the  $p(2 \times 2)\text{O}/\text{Ni}(111)$  and  $\text{Ni}(111)$  systems. The solid and dotted lines apply to the  $p(2 \times 2)\text{O}/\text{Ni}(111)$  and  $\text{Ni}(111)$  system respectively.

mized; we estimate the error in the layer growth to be 0.5 percent of a monolayer. Overlayers grown in this way produced the expected O–Ni vibration at around 70 meV. The sample was azimuthally aligned to the spectrometer scattering plane by optimizing the intensity of the  $(\frac{1}{2}, 0)$  diffraction spot.

The data for this experiment consist of energy loss spectra which were taken along the  $\bar{\Gamma}$ – $\bar{M}'$  direction in reciprocal space. In Fig. 1b we show the surface Brillouin zone for the  $p(2 \times 2)\text{O}/\text{Ni}(111)$  and  $\text{Ni}(111)$  systems. Because the  $p(2 \times 2)$  structure is unstable [9] below temperatures of 270 K, we performed these data scans at a surface temperature of approximately 300 K. The electron spectrometer was tuned to 4.5 meV resolution before each data run by examining the specular signal at the beam energy of the run. The data points were taken at equal intervals in reciprocal space, these intervals were equal to  $0.1 \zeta$  where  $\zeta \equiv Q/K_{\bar{M}}$  and  $K_{\bar{M}} = 0.729 \text{ \AA}^{-1}$ . On our HREELS spectrometer [10], the detector rotates about the crystal. The spectra taken for this experiment were acquired with respect to the incident beam impinging on the surface at a fixed angle of 60 deg with the surface normal. The energy loss spectra were taken at different points in reciprocal space by rotating the detector around the crystal axis. We were able to position the detector reliably to 0.1 deg. Finally the in-plane momentum transfer resolution was  $\pm 0.04 \text{ \AA}^{-1}$  for typical experimental configurations.

Because the probe electrons interact strongly with the surface, the scattering cross sections for the surface modes depend strongly on the energy of the incident electron beam  $E_{\text{beam}}$  and the incident orientation of this beam with the surface,  $\theta_{\text{incident}}$ . Typically most HREELS experiments require an extended search of the experimental scattering parameters,  $E_{\text{beam}}$  and  $\theta_{\text{incident}}$ , to determine configurations that optimally resolve each of the scattering modes. This experiment has been no exception. However, in this experiment we have had to contend with another variable, the quality of the overlayer surface. A  $p(2 \times 2)\text{O}$  overlayer forms on  $\text{Ni}(111)$  when a large number of islands, fed by the surrounding oxygen background, grow until they adjoin pe-

ripherally. The resulting monolayer will be composed of numerous  $p(2 \times 2)$  domains [11]. Because the domains will have correlation lengths which are smaller than those for the surface domains of the nickel substrate, scattering from the adsorbate system will contain more diffuse scattering than from only the substrate. If the adsorbate regions are particularly small this added broadening may significantly distort the energy spectrum produced by the spectrometer. Since the domain sizes will vary between surface preparations, we had to produce data sets for several overlayers for each set of incident electron scattering parameters, our goal being to produce spectra with a minimal amount of diffuse scattering. As a consequence, this experiment required a considerably large data search to produce tractable spectra. We took the data for these experiments in the region surrounding the  $(\frac{1}{2}, 0)$  diffraction spot as the signals were the most intense in this region. Kinematic conditions ( $E_i, \theta_i, \theta_f$ ) were adjusted to yield optimized signal levels for three phonon bands: the in-plane oxygen vibration, the folded Rayleigh wave and the  $S_2$  surface resonance. Signals were not optimized for the O–Ni perpendicular stretch since the  $\bar{\Gamma}$  value could be obtained under dipole allowed conditions by us and previously by others [3].

Figs. 2 and 3 show representative scans from our final data set. The spectra in Fig. 2 were taken with a beam energy of 164 eV, while the spectra in Fig. 3 used a beam energy of 160 eV. In Fig. 2 we see evidence for two lattice vibrational modes, one with an energy of approximately 17 meV at  $\zeta = 0.0$ , and another with an energy of approximately 30 meV at  $\zeta = 0.0$ . Note that both of these modes disperse throughout the surface Brillouin zone. From previous lattice studies [8], these modes would appear to be the remnant of the Rayleigh wave and the  $S_2$  mode in the original clean system. As we shall demonstrate, these modes lie within the bulk bands of the  $p(2 \times 2)\text{O}/\text{Ni}(111)$  system and are in fact surface resonance modes. The spectra in Fig. 3 were taken to reveal the oxygen vibrational modes. These peaks are not as well resolved as those from the previous set, but they indicate that the

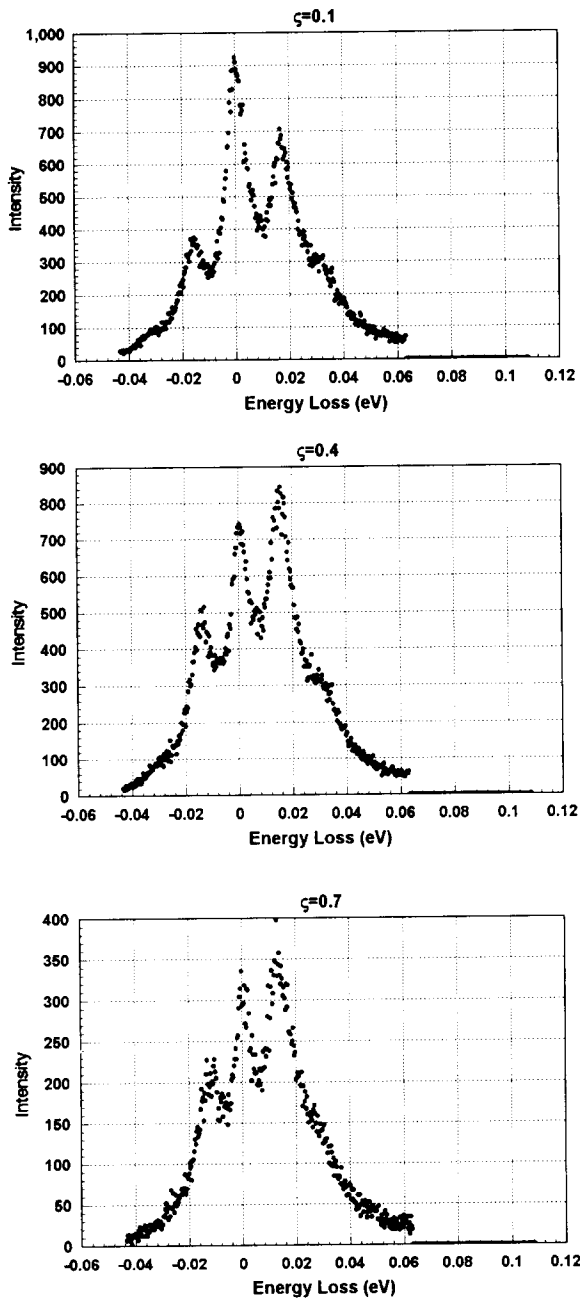


Fig. 2. Representative raw data scans at 164 eV. The label above the figure gives the momentum transfer in reduced units. Note the two dispersive modes.

oxygen mode disperses little throughout the Brillouin zone. Both sets of spectra are consistent with the original experimental data [3].

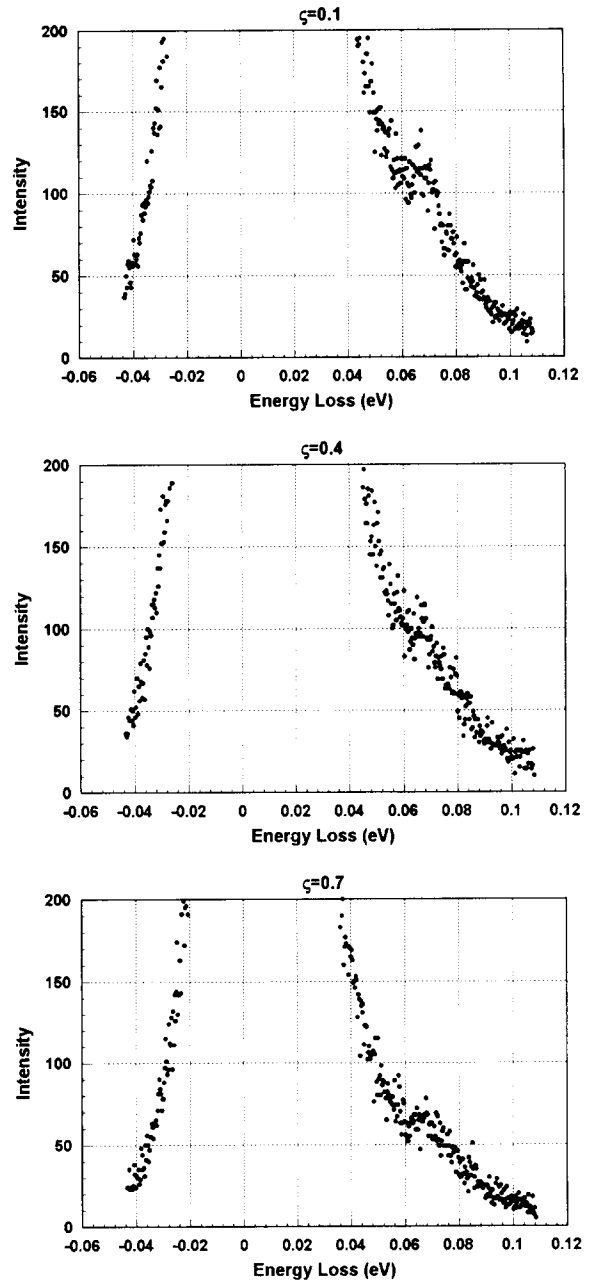


Fig. 3. Representative raw data scans at 160 eV. Again, the label above the figure gives the momentum transfer in reduced units. Note that the modes here appear to be non-dispersive.

One of the difficulties inherent in many HREELS experiments is that the resolution of the experiment tends to be large in comparison to

the spacing between the vibrational features. This coupled with the typically low signal levels implies that the experimental peaks will not have well resolved center energies. With this experiment, this problem was particularly acute as the overlayer morphology tended to add extra broadening to the spectral features while enhancing the incoherent scattering. To extract peak energies from the data we used a number of conventional maximum likelihood statistical techniques [12] to fit the data to models composed of Gaussian functions. These unfortunately did not prove sufficiently powerful; they produced peak energies that varied by several millivolts according to the initial conditions of the algorithm. To address this problem, we have developed a maximum entropy data reconstruction algorithm which we describe in the following section.

### 3. Maximum entropy analysis

The maximum entropy technique which we are using to analyze the data has philosophical roots which extend back to Laplace [13]. However, it has only been since the development of high speed computing that the technique has become practical for data analysis. The original computational and algorithmic development was accomplished by members of the astronomy community for the enhancement of spatial images. After its debut the technique has undergone a large amount of development, particularly within the past decade, and is now at the point that it has been accepted by an increasingly wide cross section of the scientific community. Recently it has been employed for extracting spectroscopic information from a complex molecular adsorption system [14].

The idea behind maximum entropy is straightforward and has been documented in a number of reviews of the subject [15]; we present the essence here. Conceptually the first step is to create a trial function which is convolved with the instrument function and then compared with the data. The trial function is essentially a set of delta functions and has as many channels as the data spectrum under analysis. The trial function

serves to represent the measured spectrum as it would appear without the distortion caused by the instrumental blurring. The parameters in this trial function are then adjusted until the convolved function is sufficiently close to the data as determined by a suitable fitting function. Then the trial function is adjusted so that its entropy is maximized while the convolved function remains a sufficiently close fit to the data. Having met these two criteria, the adjusted trial function may be taken to represent the data as it would appear without the spreading of the instrument function.

To implement this procedure mathematically we will compose a figure of merit

$$\chi^2 = \sum_{i=1}^N \left( \frac{d_i - y_i(\{x_j\})}{\sigma_i} \right)^2$$

to determine whether or not a given model spectrum is sufficiently close to the data. Here the  $d_j$  represent the measured data, the  $y_j$  are the points in the model spectrum that is produced from the convolution of the trial spectrum  $\{x_j\}$  and the  $\sigma_j$  are the variances in the data. This figure of merit is a standard statistical idea and is called chi-squared. Now we select the representative trial function by maximizing the entropy function

$$S = - \sum_i P_i \ln P_i$$

subject to the constraints

$$\sum_i P_i = 1$$

and

$$\sum_{i=1}^N \left( \frac{d_i - y_i(\{x_j\})}{\sigma_i} \right)^2 \leq N,$$

where  $P_j$  is the probability that a given signal count will appear in channel  $j$ . Here we are selecting the trial reconstruction with the maximum entropy subject to the constraints that the probabilities be normalized and that the trial function be sufficiently close to the data as determined by  $\chi^2 \leq N$ . We have implemented this algorithm with the nonlinear optimization routine from the IMSL Libraries [16]. Commercial ver-

sions of this routine also exist and are highly efficient [17].

In the description above we have not indicated the value that we have used for  $N$  in the second constraint. Traditionally this is set equal to the number of points in the spectrum, however this choice is merely a matter of convention. Our solution has been to reconstruct the spectrum for a variety of values of  $N$  and to select that value of which produces spectra with no high frequency oscillations. Typically these values lie between 1.5 and 0.9 times the number of spectral points. To determine the instrument function we scan the (0, 0) diffraction rod, that is the specular beam, and take the normalized output data for this scan to be representative of the system instrument function. We are assuming that this curve continues to be valid as we scan the spectrometer through the measurement energy range. As we are changing the analyzer energy by approximately 80 meV at maximum this is probably a valid assumption. Note also that the maximum entropy algorithm tends not to be sensitive to the details of the instrument function and changes in the shape of the instrument function will not shift the center energies of the deconvolved peaks [18].

In Figs. 4 and 5 we see the results of this algorithm as applied to the experimental data. In Fig. 4 we see that the peaks at around 17 and 30 meV are now well resolved with definite center energies, and disperse throughout the Brillouin zone as expected. Additionally we see extra peaks which appear at approximately 6 and 25 meV. We attribute the 6 meV peak to trace CO contaminants [19]; there is evidence in the lattice modeling for the 25 meV peaks which occur as a bulk band resonance. In Fig. 5 we see the results for the maximum entropy analysis of the higher lying oxygen modes. Note that we can see evidence for the two oxygen modes at  $\zeta = 0.1$ , one at around 67 meV and the other near 71 meV. The extra high lying peaks around 56 meV may be due to the oxygen occupying the second threefold site of the Ni(111) surface [23]. The other high energy peaks, around 75 and 84 meV, are probably due to trace adsorbates. In all of the maximum entropy reconstructions performed, the peak energies can be determined to an accuracy of 0.3

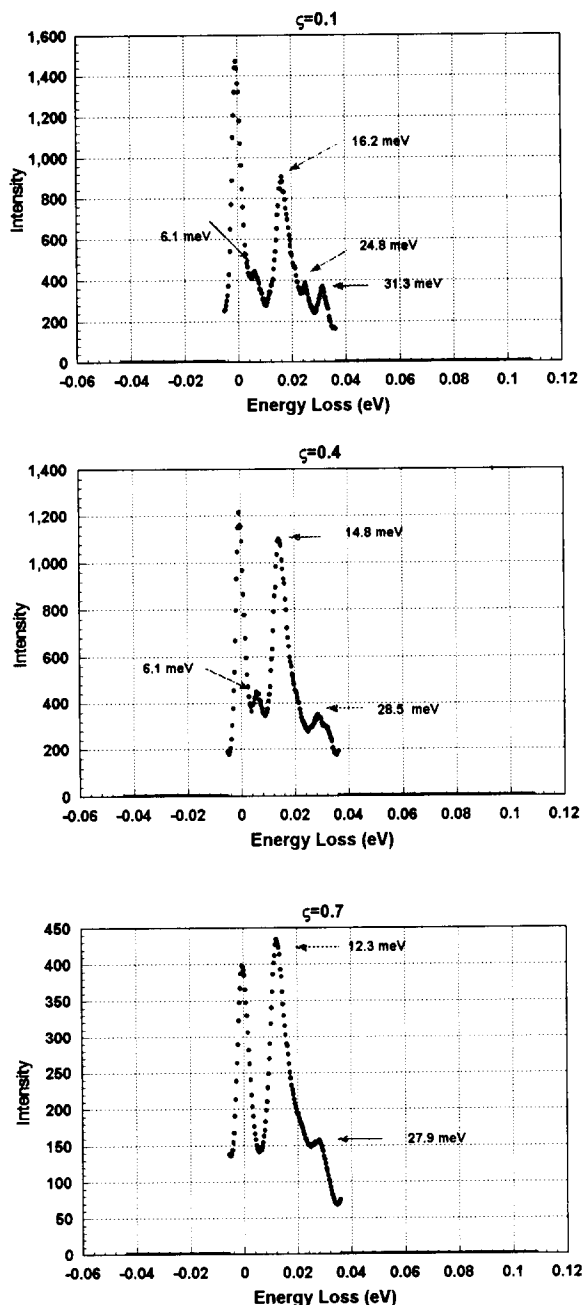


Fig. 4. Maximum entropy reconstructions of the bulk modes embedded in the 164 eV raw data of Fig. 2. The arrows give the center energies of the revealed peaks. Note that the algorithm has sharpened the existing features and has revealed new features. The error in the peak energy is 0.3 meV which is the energy scale spacing.

meV, which is the spacing of the energy scale on the multi-channel scalar that was used for spectral data acquisition.

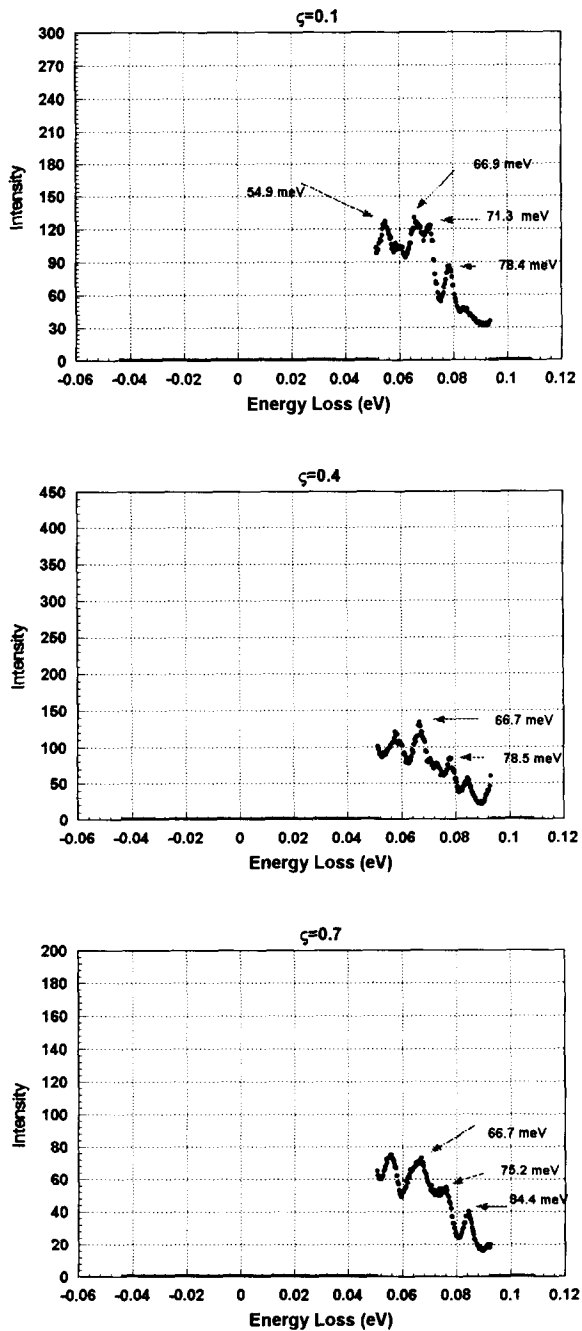


Fig. 5. Maximum entropy reconstructions of the oxygen modes embedded in the 160 eV raw data of Fig. 3.

In Fig. 6 we summarize the data for the experiment as processed by the maximum entropy routine. Here we see two dispersive modes from the bulk nickel bands, one non-dispersive mode from the oxygen vibrations and a second oxygen vibrational mode that consists of two data points. We have interpolated between these sets of points with a second-order polynomial to produce smooth curves. The respective surface Brillouin zone center energies for the nickel modes are 16.9 and 31.8 meV, the latter number being an extraction from 7 eV data. These are in reasonable agreement with the previous study [3]. The lower oxygen mode intersects at around 67 meV, the upper at around 70 meV. We have included the two points from the 25 meV bulk mode extracted with maximum entropy, we omit the points from the 6 meV mode as they may be due to trace CO adsorption.

#### 4. Lattice dynamical calculations

Having now extracted spectroscopic data from the system, we would like to connect it with a lattice model to develop an understanding of the surface force field. Typically, in vibrational studies such as this one, a simplified lattice model is constructed to serve as a framework for interpreting the data. A set of initial values are assigned to the model parameters and then these parameters are adjusted until the model fits the data.

The first step in this process is to develop the model so that it describes the bulk phonons. In this experiment we will be interested in the salient differences between the surface bonds and those in the bulk. Consequently, we will employ a single force constant model to describe the bulk phonons. This model captures the essential features of the bulk crystal system while it omits details which will not be evident in our scattering data. We will set the value of the force constant to  $3.79 \times 10^4$  dyn/cm; this choice has been shown [20] to provide a reasonable fit to the bulk dispersion curves.

As we have indicated in a previous section, and as has been shown by the recent study by Grimsby et al. [2], the oxygen overlayer serves to

reconstruct the original Ni(111) surface substantially. The challenge we had to face with this particular system has been to describe the system behavior with a model that captures the essential features of the system while remaining tractable. In consequence, we have focused upon the system geometry as the defining feature of the system, and have kept the bond model simple – bonds between two atoms will be nearest neighbor bonds described with a single parameter. Even given this simplification we still need a total of 8 parameters to describe the surface interactions; these are illustrated in Fig. 7. This figure labels respectively the different bonds within the first layer and the different bonds between the first and second layers. The bulk bond is labeled as bond type 1 while the oxygen to nickel bond is labeled as bond type 2. We have assumed that the remaining bonds have their bulk value.

With the bond geometry now established, we need to develop a model for the system bond strengths. Our approach will be to describe these bonds with a simple scaling relation and use these scaled force constants as the starting point for our lattice model. We are led to this choice both because the system is complex and needs to be

interpreted in light of some simplifying assumptions and because the scaling models which we are using have been successful in a wide range of situations. To wit, we will use the relation

$$\frac{f_s}{f_b} = \left( \frac{r_b}{r_s} \right)^\alpha,$$

where  $r_b$  and  $r_s$ , are respectively bulk and surface bond lengths,  $f_b$ , and  $f_s$ , are the force constants associated with those bonds and  $\alpha$  is an adjustable parameter. This relation was first proposed by Badger [21,22] for understanding the bond structure in molecules and has subsequently been employed to model surface systems in a number of instances [23]. These relationships developed by Badger provide a succinct mathematical expression for the empirical correlations which exist between force constants and bond lengths in a large number of chemically interacting systems.

In Table 1 we present the bond lengths for the bonds labeled in Fig. 7. Note that there are two different bond lengths for the bonds that we have labeled as 8. The difference between these lengths is sufficiently small that we will consider all of the bonds labeled 8 to be effectively identical to reduce the complexity of the model. Now we

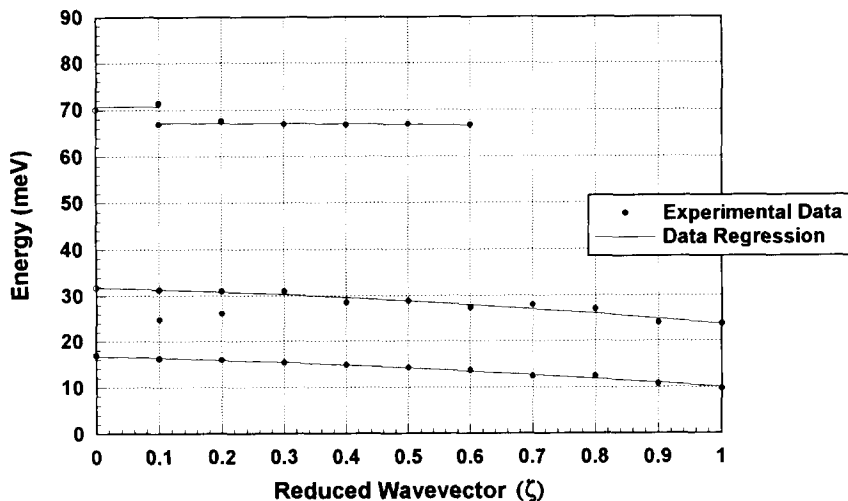


Fig. 6. Dispersion curves constructed with the results of the maximum entropy reconstructions. The data regression is a second-order polynomial fit to the data. The lower lying modes around 16 and 30 meV are excitations of the nickel bulk bands while the mode around 67 meV and the point at around 71 meV due to oxygen adsorbate vibrations. The two points at 26 meV are also potentially due to a bulk mode. An open circle curve marker indicates that a particular point was extracted from data taken at an incident beam energy of 7 eV.

need to choose a value for  $\alpha$ . In a number of studies covering different types of metals [24], values between 7 and 8 have provided reasonable fits to the data. We will therefore take  $\alpha$  to have the value 7.5. In Table 2 we show the surface force constants as produced by the scaling relation. These numbers will serve as the starting point for our computations.

To study the lattice dynamics of the system we have formed a 30 layer slab, computed the dynamical matrix, and solved this for the eigenvalues and eigenvectors. The surface phonon energies converge once the slab has reached 10 layers of thickness.

The output of the eigenenergies for this slab calculation are presented in Fig. 8. Two distinct

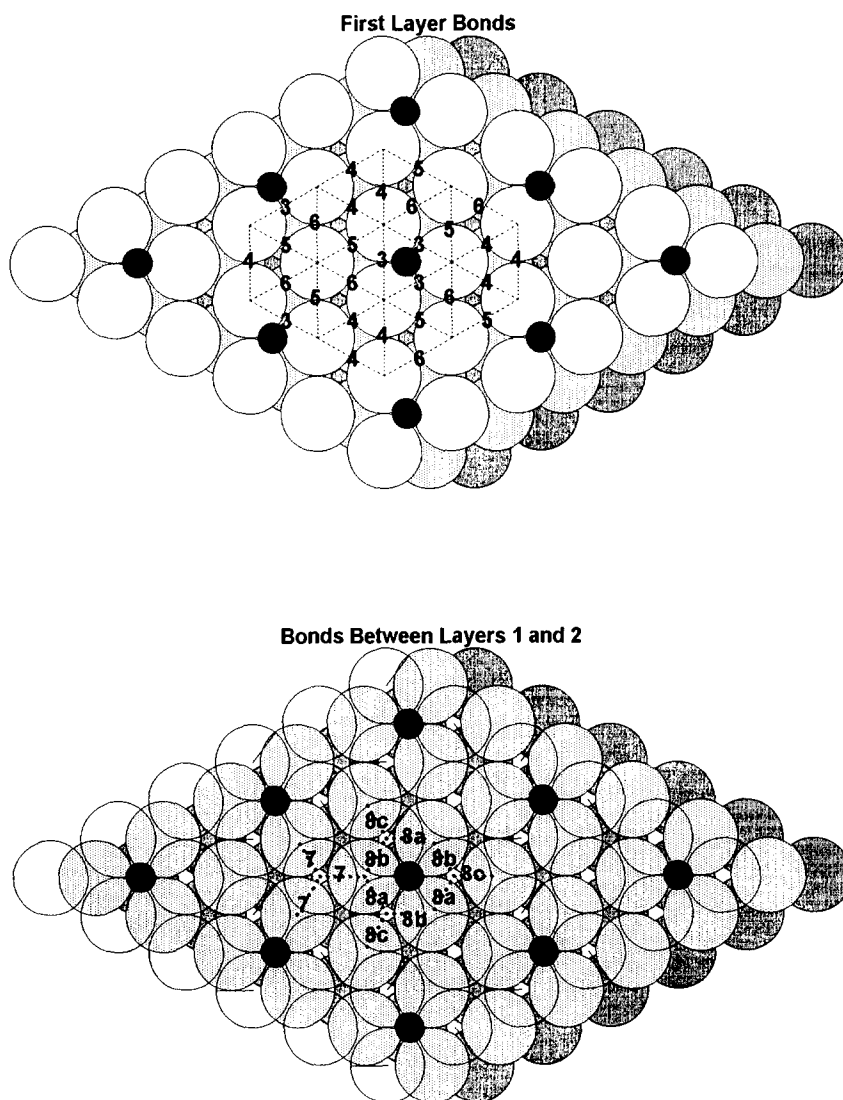


Fig. 7. The system bonds as dictated by our modeling effort. The upper figure labels the bonds between the first layer nickel atoms while the lower figure labels the bond between the unit cell atoms and the nickel atoms in the second layer. To simplify the model the bonds labelled 8 have been treated as identical. The oxygen to nickel bond we have labelled as bond 2; the remaining bonds have the bulk value and are bond 1.

Table 1  
Bond lengths as deduced from the structural model proposed by Grimsby et al. [2]

Type 1	2.49 Å
Type 2	1.83 Å
Type 3	2.55 Å
Type 4	2.43 Å
Type 5	2.56 Å
Type 6	2.43 Å
Type 7	2.42 Å
Type 8a	2.57 Å
Type 8b	2.59 Å
Type 8c	2.57 Å

oxygen modes and a set of bulk bands are apparent. The bulk bands arise because the surface breaks the translational symmetry of the crystal. Electrons scattering from the crystal still must conserve their wavevectors in the two directions parallel to the surface, however in the direction normal to the crystal surface the wavevector need not be conserved. Consequently there will be a large number of possible energies for a given wavevector; these energies form the bulk continuum.

Table 2  
Force constants generated from the scaling model described in the text

Type 1	$3.79 \times 10^4$ dyn/cm
Type 2	$22.0 \times 10^4$ dyn/cm
Type 3	$3.17 \times 10^4$ dyn/cm
Type 4	$4.55 \times 10^4$ dyn/cm
Type 5	$3.07 \times 10^4$ dyn/cm
Type 6	$4.55 \times 10^4$ dyn/cm
Type 7	$4.69 \times 10^4$ dyn/cm
Type 8	$2.99 \times 10^4$ dyn/cm

Because of the reduced size of the reciprocal unit cell, the surface dispersion curves do not always exhibit pure surface modes as typically found in clean metal systems but rather can be surface resonances which scatter electrons strongly. To locate these surface resonances we will employ a standard lattice dynamical technique [25]. This method involves examining the spectral density curves for the top layers of the sample. These curves are given by the expression

$$\pi(\gamma, \mathbf{k}_2, \omega) = \sum_s [\epsilon_s(\gamma, \mathbf{k}_2)]^2 \delta[\omega - \omega_s(\mathbf{k}_2)],$$

where  $\gamma$  stands for the coordinates of a particular atom in the unit cell,  $\mathbf{k}_2$  is the two-dimensional

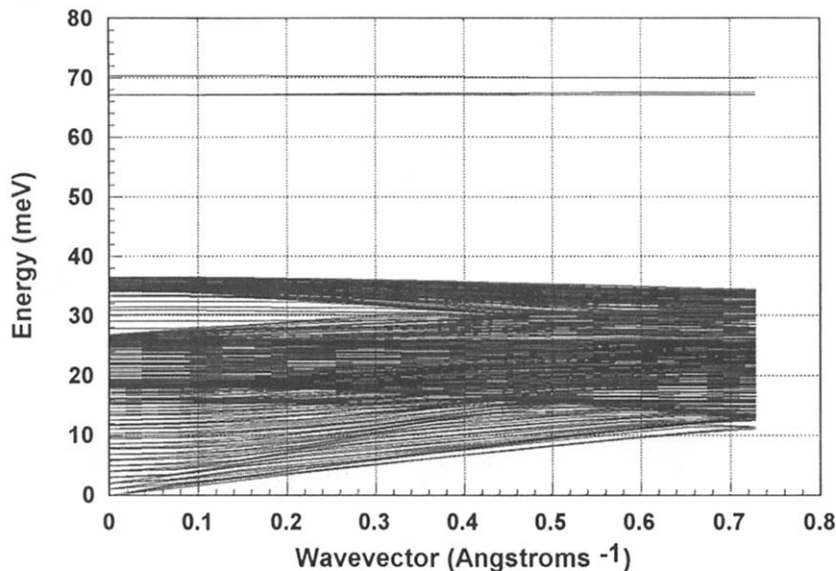


Fig. 8. Dispersion curves for  $p(2 \times 2)\text{O}/\text{Ni}(111)$  produced by a 30 layer slab calculation. Note that the wavevector units here are absolute rather than normalized. The dispersion curves extend to the edge of the surface Brillouin zone for the  $p(2 \times 2)\text{O}/\text{Ni}(111)$  system.

phonon wave vector,  $\omega$  is the phonon energy,  $\epsilon_s$  is one of the system dynamical eigenvectors and  $\omega_s$  is the eigenvalue for the particular eigenvector. Our working assumption is that the surface resonances will appear in the spectral density curves as sharp features and that we may assign these features to modes in the data. These ideas grew out of early scattering theories that are

based upon the Born approximation. These theories do not give correct quantitative cross sections for inelastic electron scattering, however they do enable us to locate the surface resonances.

Two typical spectral density curves for the  $p(2 \times 2)\text{O}/\text{Ni}(111)$  system are shown in Fig. 9, the former applies to the oxygen atom while the latter applies to the first layer nickel atom not

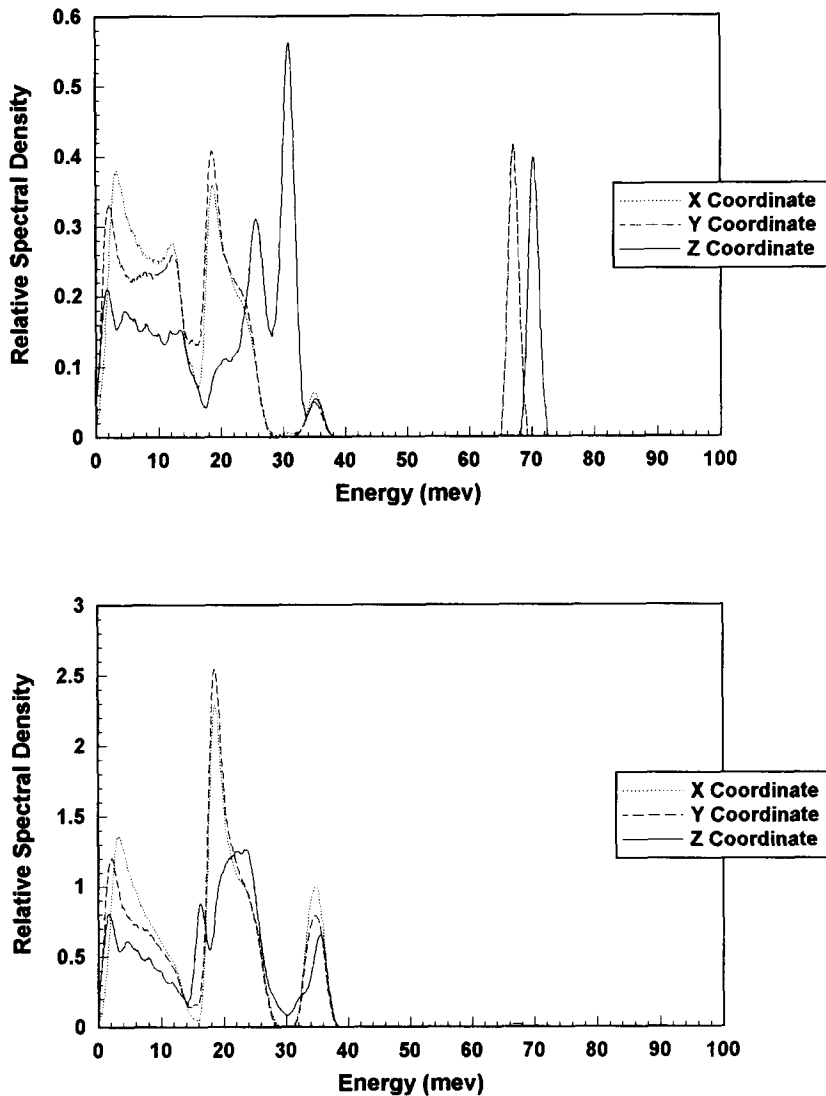


Fig. 9. Representative spectral density curves produced by the lattice model. The upper figure represents spectral density curves for the oxygen atoms while the lower figure shows these curves for the nickel atom in the first unit cell not bonded to the oxygen atom. These particular curves apply at the Brillouin zone center. The  $z$  direction is normal to the surface, the  $z$  and  $x$  directions define the scattering plane and the  $y$  direction is normal to the  $x$  and  $z$  directions.

bonded to the oxygen atom. These curves both apply for  $\zeta = 0.0$ . Note that there are a number of sharp features which are indicative of surface resonances. There are also the oxygen vibrational modes which are evident around 67 and 71 meV in Fig. 8. These are true surface modes as they do not mix with the bulk vibrations. Additionally in Fig. 9 we see a resonance feature around 30 meV; this corresponds to the  $S_2$  mode remnant as we indicated previously. We also see another feature which appears around 24 meV; at this energy there is a large contribution from the bulk density of states and these are probably responsible for the maximum entropy resolved peak at this energy. Finally in the lower section of Fig. 9 there is a sharp feature in the  $z$  coordinate around 16 meV. This is the remnant of the Rayleigh mode for the clean system. For increasing wave vector, the sharp features become less well defined until at around  $\zeta = 0.4$  they lose their delta function character and do not have well defined center energies.

In this study we calculated spectral density curves for a large number of trial parameter sets. For each of these sets of lattice parameters, we

calculated spectral density curves for each of the atoms in the top four layers of the unit cell along the  $\bar{\Gamma}-\bar{M}'$  direction in reciprocal space. Considering a complete set of curves for a given parameter set, we find that the spectral density curves for the oxygen atom and the non-oxygen bonded nickel atom are sufficient to locate all of the salient modes of the system. Further, these salient features persist as we vary the parameters of the model. Consequently we have concluded that these sharp features are valid choices for the scattering modes. Note also that these results are consistent with the surface Brillouin zone center phonons developed by the earlier theoretical lattice studies [4–7].

The sharp resonances and oxygen surface modes produced by the theory match the data well. Consequently we will associate the theoretical modes which exist at around 16, 30, 67 and 71 meV in the center of the surface Brillouin zone with the corresponding modes in the data, confirming our earlier assignments. Note that we have also acquired a feature at 24 meV, but as we have relatively few experimental points we have not included this mode in our analysis.

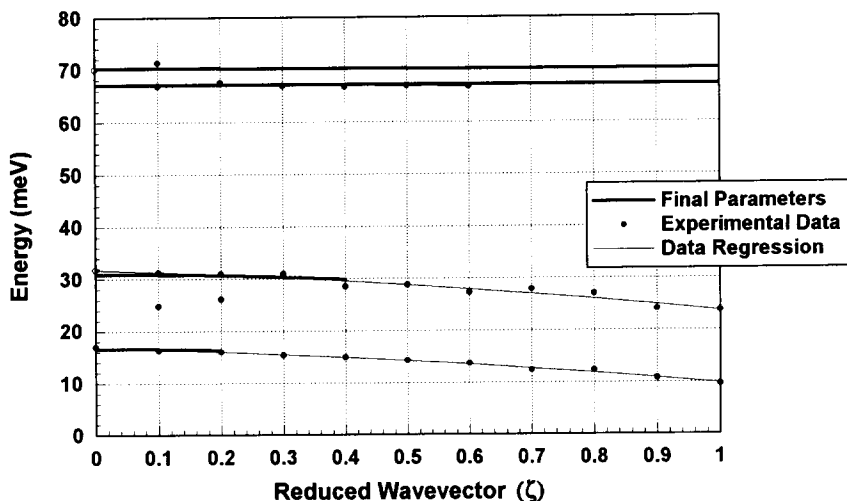


Fig. 10. Theoretical dispersion curves added to the experimental dispersion curves. The theoretical dispersion curves have been extracted from the spectral density curves and are denoted as heavy lines in the figure. The force constants used to generate the theoretical curves are those listed in Table 2. Note that we have not extended the two lower lying theoretical dispersion curves throughout the entire Brillouin zone. These curves are surface resonances and do not produce sharp spectral density features at large wavevector with well defined center energies.

Finally we have adjusted the lattice parameters to fit the data. We have created a lattice model using the force constants listed in Table 2. From this lattice model and its associated spectral density curves we have produced a set of theoretical dispersion curves which we show in Fig. 10, along with the experimental data points. Note that the fit for this model is good. To understand the sensitivity of the observed modes to changes in the model lattice parameters, we perturbed each of the parameters in turn by 20 percent in both the positive and negative directions. Except for parameters 5 and 6, whose variation changed the model little, changes in the other force constants produced variations in the mode energies of approximately 1.0 meV; changes in parameter 2 influence the oxygen modes, changes in parameters 3 and 4 affect the 30 meV mode, changes in parameter 7 affects the 16 meV mode and changes in parameter 8 affect both modes.

The conclusion from the perturbation study is that the original set of scaled parameters with no modification provides a very good fit to the system data. Given that our data are accurate to 0.3 meV, we can conclude that the scaling model parameters are accurate to about 20 percent.

## 5. Conclusions

In this paper we have analyzed the surface force field for  $p(2 \times 2)\text{O}/\text{Ni}(111)$  in order to quantify the modifications that oxygen adsorption induces on Ni–Ni bonding interactions in the interfacial region of this system. A powerful maximum entropy deconvolution algorithm was used to extract enhanced surface phonon spectroscopic data from inelastic electron scattering measurements taken along the  $\bar{\Gamma}-\bar{M}'$  direction. This use of this algorithm was quite beneficial for analyzing the scattering data from this interface due to the complex domain structure, and consequent diffuse scattering characteristics of this system.

A lattice dynamical model was then constructed in which the Ni–Ni bonding interactions were given by a scaling relation which relates intermetallic force constants to bond length in which the various bond lengths present in the

surface region were referenced to a single force constant description of the bulk Ni–Ni interaction. The dispersion curves resulting from this lattice dynamics calculation, which used as input the recent structural assignment of Grimsby et al. [2], provide an excellent description of the experimental data.

The surface force field derived in this way for  $p(2 \times 2)\text{O}/\text{Ni}(111)$  differs significantly from that of the clean Ni(111) interface. Most notably, oxygen adsorption induces geometric change in the topmost layers, i.e., the surface reconstructs, and in so doing apparently relieves the surface stress present on the clean metal as it is not required in the lattice model.

That the bonding interactions follow a scaling rule is reasonable in retrospect. Scaling rules have been used in many cases to treat systems as collections of localized bonds. They were first developed by R. Badger for describing diatomic [21] and polyatomic [22] molecules and have been employed recently to understand solid surfaces [23]. The results presented herein are interesting as they indicate that under proper circumstances a relatively simple local bonding model can provide an adequate description for the forces present at chemically modified metallic surfaces.

## Acknowledgments

This paper has been submitted by Glenn Tisdale in partial fulfillment of the doctoral degree requirements of the Department of Physics at The University of Chicago. This work was supported, in part, by the Air Force Office of Scientific Research, Grant Nos. AFOSR-88-0194 and AFOSR-F49620-93-1-0044; by the Department of Defense University Research Instrumentation Program; and by the National Science Foundation Materials Research Laboratory at the University of Chicago. The authors also would like to express their gratitude to numerous colleagues. These include W. Menezes, P. Knipp, J.S. Ha and K. Gibson. They would also like to thank H. Krebs and D. Smith for invaluable technical assistance. Fruitful discussions with J.E. Black regarding lattice dynamical calculations are gratefully

acknowledged. Finally, L. Kesmodel and LK Technologies are thanked for numerous technical discussions dealing with electron spectrometers.

## References

- [1] P.M. Marcus, J.E. Demuth and D.W. Jepsen, *Surf. Sci.* 53 (1975) 501.
- [2] D.T. Vu Grimsby, Y.K. Wu and K.A.R. Mitchell, *Surf. Sci.* 232 (1990) 51.
- [3] H. Ibach and D. Bruchmann, *Phys. Rev. Lett.* 44 (1980) 36.
- [4] G. Allan and J. Lopez, *Surf. Sci.* 95 (1980) 214.
- [5] V. Bortolani, A. Franchini, F. Nizzoli, G. Santoro, *Solid State Commun.* 41 (1982) 369; *J. Electron Spectrosc. Relat. Phenom.* 29 (1983) 219.
- [6] J.E. Black, *Surf. Sci.* 100 (1980) 555; in: *Vibrations at Surfaces*, Eds. R. Caudano, R. Gilles and A.A. Lucas (Plenum, New York, 1981).
- [7] R.L. Strong and J.L. Erskine, *Phys. Rev. B* 31 (1985) 6305.
- [8] W. Menezes, P. Knipp, G. Tisdale and S.J. Sibener, *Phys. Rev. B* 41 (1990) 5648; *J. Electron Spectrosc. Relat. Phenom.* 54/55 (1990) 373.
- [9] A.R. Kortan and R.L. Park, *Phys. Rev. B* 23 (1981) 6340.
- [10] L.L. Kesmodel, *J. Vac. Sci. Technol. A* 1 (1983) 1456.
- [11] P.H. Holloway and J.B. Hudson, *Surf. Sci.* 43 (1974) 141.
- [12] W. Press, *Numerical Recipes* (Cambridge Univ. Press, New York, 1986).
- [13] E.T. Jaynes, in: *Maximum Entropy and Bayesian Methods*, Ed. J. Skilling (Kluwer, New York, 1989).
- [14] Y. Wang and W. Henry Weinberg, *Phys. Rev. Lett.* 69 (1992) 3326.
- [15] B. Buck and V. Macaulay, Eds., *Maximum Entropy in Action* (Oxford Univ. Press, Oxford, UK, 1991).
- [16] IMSLMATH Library Ver 1.0 (Visual Numerics, Dallas, TX, 1991).
- [17] S. Gull and J. Skilling, *MEMSYS 3 Users' Manual* (Maximum Entropy Data Consultants Limited, Royston, UK, 1989).
- [18] A.I. Grant and K.J. Packer, in: *Maximum Entropy and Bayesian Methods*, Ed. J. Skilling (Kluwer, New York, 1989).
- [19] J.S. Ha and S.J. Sibener, *Surf. Sci.* 256 (1991) 281.
- [20] R.J. Birgeneau, J. Cordes, G. Dolling and A.D.B. Woods, *Phys. Rev.* 136 A (1964) 1359.
- [21] R.M. Badger, *J. Chem. Phys.* 2 (1934) 128.
- [22] R.M. Badger, *Phys. Rev.* 48 (1935) 284.
- [23] H. Ibach and D.L. Mills, *Electronic Energy Loss Spectroscopy and Surface Vibrations* (Academic Press, New York, 1982).
- [24] A.P. Baddorf, I.W. Lyo, E.W. Plummer and H.L. Davis, *J. Vac. Sci. Technol. A* 5 (1987) 782; P. Zeppenfeld, K. Kern, R. David, K. Kuhnke and G. Comsa, *Phys. Rev. B* 38 (1988) 12329.
- [25] T.S. Rahman, J.E. Black and D.L. Mills, *Phys. Rev. B* 25 (1982) 883.